

## Sources and holes in a one-dimensional traveling wave convection experiment

Luc Pastur,<sup>1</sup> Mark-Tiele Westra,<sup>1</sup> Daniel Snouck,<sup>1</sup> Willem van de Water,<sup>1</sup> Martin van Hecke,<sup>2</sup> C. Storm,<sup>3</sup> and Wim van Saarloos<sup>3</sup><sup>1</sup>Physics Department, Eindhoven University of Technology, Postbus 513, 5600 MB Eindhoven, Netherlands<sup>2</sup>Kamerlingh Onnes Laboratory, Universiteit Leiden, Postbus 9504, 2300 RA Leiden, Netherlands<sup>3</sup>Instituut-Lorentz, Universiteit Leiden, Postbus 9506, 2300 RA Leiden, Netherlands

(Dated: January 10, 2022)

We study dynamical behavior of local structures, such as sources and holes, in traveling wave patterns in a very long (2 m) heated wire convection experiment. The sources undergo a transition from stable coherent behavior to erratic behavior when the driving parameter  $\beta$  is decreased. This transition, as well as the scaling of the average source width in the erratic regime, are both qualitatively and quantitatively in accord with earlier theoretical predictions. We also present new results for the holes sent out by the erratic sources.

PACS numbers: 47.20.Bp, 47.20.Dr, 47.54.+r, 07.05.Kf

Traveling wave systems play an exceptional role within the field of pattern formation. If the transition to patterns is supercritical (forward), the dynamics close to threshold should be amenable to a description by the Complex Ginzburg-Landau (CGL) amplitude equation [1]. Theory and experiments are difficult to compare, however, for the following two reasons: (i) both the CGL model and experimentally observed traveling wave patterns exhibit an astonishing variety of ordered, disordered and chaotic dynamics, which can be difficult to characterize or compare. (ii) The dynamics depends, in general, strongly on non-universal coefficients [2, 3, 4], but the values of these coefficients are difficult to determine in experiments [5, 6, 7].

The study of local structures, such as sources, fronts and holes which play an important role in traveling wave systems [1, 2, 3, 4, 7, 8, 9, 10, 11, 12], provide a promising route to compare theory and experiment as they partially circumvent these difficulties: their nontrivial behavior often depends only on a subset of the coefficients [11] and is, in addition, relatively easy to characterize experimentally [7, 8, 9, 12].

In this paper we present a successful example of this approach in a heated wire convection experiment (Fig. 1). This system forms left and right traveling waves that suppress each other; typical states consist of patches of left and right traveling waves, separated by sources (which send out waves) and sinks (which have two incoming waves) [13]. Earlier theoretical work [14], which was based on the amplitude equations (1-2) below, predicts that, essentially due to the transition from an absolute to a convective instability [15], sources tend to display a diverging width when the driving parameter  $\beta$  is lowered beyond a critical value [Eq. (3)]. More recently it was predicted that just before these stationary sources would diverge, they become unstable and give way to fluctuating sources of finite average width which display highly non-trivial dynamics [4].

We indeed observe this nontrivial change in source be-

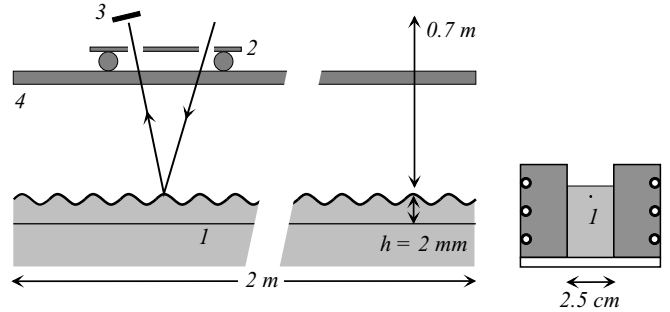


FIG. 1: Schematic side-view and cross section of the heated wire experiment. A thin (0.2 mm diameter) wire (1) is stretched beneath the free surface of a fluid (depth  $h = 2$  mm). When it is heated by sending an electrical current through it, surface waves are excited. The slope of the waves is measured by reflecting a laser beam on the surface onto a position sensitive detector (PSD) (3). The laser and the PSD are mounted on a cart (2) that rides on precision steel rods (4).

havior when the driving (heating of wire) is decreased; not only the measured transition value, but also the qualitative behavior of sources is in accord with the predictions [4, 14]. All properties necessary to compare theory and experiment are measured in a set of independent experiments. The fluctuating sources send out holes, and we show that these display behavior very similar to that predicted for homoclinic holes [3].

## I. EXPERIMENTAL SETUP

Our experiment consists of a 2 m long heated wire of diameter of 0.2 mm and resistivity of  $50 \mu\Omega/\text{m}$  that is placed under the free surface of the fluid at a depth  $h = 2$  mm (see Fig. 1). The wire is stretched to the breaking limit and its maximum sagging is 0.1 mm. The heat  $Q$  dissipated in the wire drives the system; through

a combination of gravity- and surface tension induced convection, surface waves emerge at  $Q = Q_c$  that travel along the wire [12]. The sides of our cell are made of brass and contain copper tubes through which cooling water of  $21.0 \pm 0.1$  C is circulated. In order to guarantee a clean, uncontaminated free surface, we use a low-viscosity, low-surface-tension silicon oil [16].

A sensitive linear measurement of the surface slope along the cell is obtained by recording the reflection of a laser beam off the fluid surface onto a position sensitive device. Both laser and position detector are mounted on a computer-controlled cart which travels on precision stainless steel rods. This allows us to measure surface wave amplitudes as small as  $0.5 \mu\text{m}$ . The signals of the scanning device are wave frequency and Hilbert transformed to yield the complex valued field  $A(x;t) = \tilde{A} j \exp(i\phi)$ . From this the local wave number is computed as  $q(x;t) = \partial \phi(x;t) / \partial x$ . To improve the signal to noise ratio, running averages over a time interval of 10 s are performed.

Vince and Dubois [12] already demonstrated that the primary bifurcation at  $Q = Q_c$  is supercritical and explored the phase diagram as a function of  $Q$  and wire depth  $h$ . For  $\epsilon < 0.15$  the amplitude exhibits the scaling  $\tilde{A} j \propto \epsilon^{1/2}$ . This is expected near a supercritical bifurcation, and it also sets the range of applicability of the amplitude description.

## II. AMPLITUDE EQUATIONS

For systems with counter-propagating waves, the appropriate amplitude equations are the coupled one-dimensional CGL equations [1]:

$$\partial_t A_R + s_0 \partial_x A_R = \mu A_R + \frac{2}{0} (1 + ic_1) \partial_x^2 A_R + \mathcal{G}(1 - iq) \tilde{A}_R \tilde{A}_R + \mathcal{G}(1 - iq) \tilde{A}_R \tilde{A}_L; \quad (1)$$

$$\partial_t A_L + s_0 \partial_x A_L = \mu A_L + \frac{2}{0} (1 + ic_1) \partial_x^2 A_L + \mathcal{G}(1 - iq) \tilde{A}_L \tilde{A}_L + \mathcal{G}(1 - iq) \tilde{A}_L \tilde{A}_R; \quad (2)$$

Here  $A_R$  and  $A_L$  are the amplitude of the right and left moving waves,  $s_0$  is the linear group velocity, and  $c_1; c_2$  and  $c_3$  measure the linear and nonlinear dispersion. The experimentally accessible control parameter  $\epsilon$  measures the distance from threshold. The coefficients  $0; 0$  and  $g_0$  give the scales of time, space and amplitude. To model our experiment, where left and right traveling waves suppress each other,  $g_2$  should be larger than  $g_0$  [4].

### A. Scaling

Sources show complicated behavior within the amplitude equations (1-2) [4, 14]. For

$$\epsilon > \epsilon_c^{so} > \epsilon_{ca} = \frac{(s_0 - 0)^2}{4(1 + c_1^2)} \quad (3)$$

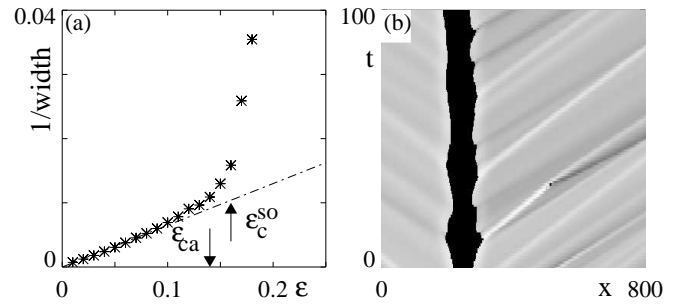


FIG. 2: Numerical results for the behavior of sources in the coupled amplitude equation (1), (2). (a) Inverse average source width as a function of  $\epsilon$ , for the coupled CGL equations with  $s_0 = 1.5; c_1 = 1.7; c_2 = 0; c_3 = 0.5; g_0 = 1$  and  $g_2 = 2$ . The coefficients  $s_0$  and  $c_1$  were chosen to be similar to those measured in the experiment; also  $g_2 > g_0$  in the experiment. The values of  $c_2$  and  $c_3$  were chosen such that the plane waves remain stable; their precise value does not play a significant role then. Note the crossover near  $\epsilon_{ca} = 0.14$ . (b) Space-time plot of the local wave number of a fluctuating source for  $\epsilon = 0.11 < \epsilon_c^{so} = 0.14$ , illustrating fluctuations of the width. In the black region the amplitude has fallen below 10% of the saturated value; the light and dark curves correspond to hole-like wave number packets sent out by the source.

sources are coherent structures with a well-defined shape, while for  $\epsilon < \epsilon_c^{so}$  sources start to fluctuate and their average width scales as  $\epsilon^{-1}$  (see Fig. 2). The quantity  $\epsilon_{ca}$  in Eq. (3) is simply the value of  $\epsilon$  where the transition from absolute to convective instability of the  $A = 0$  state occurs [14, 15]; its relevance can be understood as follows. Consider the dynamics of a single front in the left-moving wave amplitude  $A_L$  only, for which  $A_L(x=1) \neq 0$ . The propagation velocity of this front is given by a competition between the linear group-velocity, which tends to convect any structure to the left with velocity  $s_0$ , and the propagation of the front into the  $A = 0$  state with, in the comoving frame, velocity  $v = 2 \frac{0}{0} (1 + c_1^2) = 0$  [4, 14]; the front velocity in the lab frame is thus  $v = s_0$ . Viewing a source as a pair of fronts in  $A_L$  (on the left) and  $A_R$  (on the right), it is clear that these fronts move together when  $\epsilon > \epsilon_{ca}$ , but move apart when  $\epsilon < \epsilon_{ca}$ ; the change in direction of front propagation precisely corresponds in the transition from absolute to convective instability.

Numerical simulations of Eq. 1 were done in order to see whether the experimentally observed source behavior described below could be understood on basis of the amplitude description. Such simulations [4] have revealed that sources do not simply move apart and diverge when the instability of the  $A = 0$  state becomes convective; for  $\epsilon = \epsilon_c^{so} > \epsilon_{ca}$ , when the sources have become very wide, they start to fluctuate. For smaller  $\epsilon$ , the average source width scales as  $\epsilon^{-1}$  (see Fig. 2). The mechanism responsible for the sources staying at a finite but large average width is not completely understood and may depend on the noise strength. In the low noise limit, the "tip" regions of the two fronts sense the other mode which leads

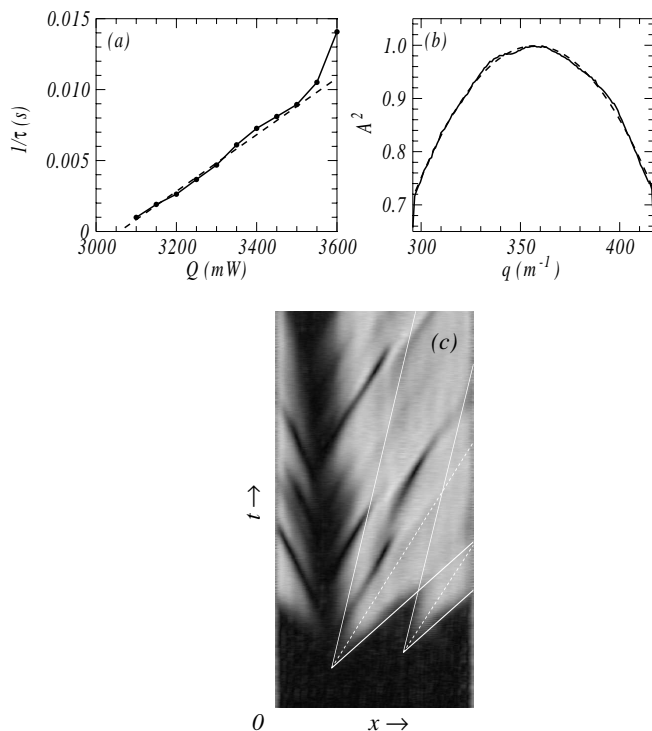


FIG. 3: Determination of the coefficients of the CGLE. (a) Time scale determined from the exponential growth of the amplitude in quench experiments for various values of the heating power  $Q$ . This time scale as  $l/\tau = \tau_0^{-1}$ , with  $\tau_0 = 16(1)$  s. (b) Correlation length  $l_0$ . Full line: histogram of squared modulus  $A^2$  vs  $q$  which is measured from a modulated wave field at  $\mu = 0.10$ . Dashed line:  $l_0^{-2} = \tau_0^{-2} = (c_1 q_0)^{-2}$ , with  $c_1 = 2.7(6) \cdot 10^3$  m.  $A^2$  is normalized so that  $A^2 = 1$  corresponds to waves with wave number  $q_0$ . (c) Front velocity. Shown is the modulus  $A(x;t)$ . The  $x$  extent of the scan is 0.682 m, the total time is 5242 s. At  $t = 0$  the power is quenched from  $Q = 0$  to  $Q = (1 + \mu)Q_c$ , with  $\mu = 0.051$ . The white lines outline two fronts. Since  $\mu < \mu_{ca}^{(0)}$  here, both fronts propagate in the same direction (here to the right).

to the formation of phase slips there. The resulting perturbations are then advected by the group-velocity and amplified by the linear growth-rate, resulting in a jittery motion of the front. For larger noise strength, convective amplification of noise may compete with this mechanism.

These phenomena are illustrated in Fig. 2 which has been calculated for parameter values which are in the range of the experimental ones, but we emphasize that the predicted source instability is generic and insensitive to the precise parameter values.

### III. MEASUREMENTS

#### A. Front and group velocities

Now that we have discussed the theoretical predictions for sources, we return to our experiment. For a compar-

ison of the source behavior with theory, we need to determine the transition from convective to absolute instability, which requires measurements of the group velocity and the front velocity as function of  $\mu$ .

The group velocity  $s_0$  was determined from the propagation of deliberate perturbations of the surface. We found that it has the same sign as the phase velocity and that it shows only a weak  $q$  dependence, so we associate the measured value  $2.1(1) \cdot 10^4$  m  $s^{-1}$  with the linear group velocity  $s_0$ .

Fronts were made by quenching the heating power  $Q$  to a finite value  $Q = (1 + \mu)Q_c$  at  $t = 0$ . After a short while, waves invade the unstable surface in the form of fronts. The boundaries of these fronts travel with  $s_0$  and  $v_f$  respectively, where  $v_f$  scales with  $\mu$  as  $v_{f0} \mu$ . Fig. 3c shows the evolution of the amplitude of the waves for  $\mu = 0.051$ ; this value appears to be below  $\mu_{ca}$  because the velocity of the fronts has the same sign as the group velocity. The results of several experiments, both at  $\mu < \mu_{ca}$  and  $\mu > \mu_{ca}$  yields that  $v_{f0} = 5.4(5) \cdot 10^4$  m/s. Comparing this to the value obtained for  $s_0$ , we immediately find that  $\mu_{ca} = 0.15(5)$ . An alternative estimate of  $\mu_{ca}$  was made from observing at which  $\mu$  the slowest moving edge of a front has zero velocity, which led to a value of  $\mu_{ca} = 0.10(2)$ .

#### B. Measurements of the coefficients

In principle, a confrontation of theory and experiment can also be performed by measuring the characteristic time ( $\tau_0$ ) and length ( $l_0$ ) scales, the linear group velocity  $s_0$  and linear dispersion coefficient  $c_1$ , since from these the transition from convective to absolute instabilities also follows (see Eq. 3). Note that starting from the full hydrothermal equations, these coefficients can in principle be obtained from a systematic amplitude expansion [1]. At present, we can only obtain  $c_1$  via measurements of the front-velocity which leads to a consistency check (see below). The length and time scales are relevant for comparing spacetime diagrams of experiment and theory and are measured independently.

The characteristic time is determined from measurements in which the growth of the amplitude is followed when, after a sufficient long transient in which a plane wave is established,  $\mu$  is increased from  $\mu = 0.017$  to larger values. The initial growth of  $A^2$  is exponential  $\exp(t/\tau)$ , and repeating this experiment for various values of  $\mu$  yields the data presented in Fig. 3. Using that  $l/\tau$  scales as  $l/\tau = \tau_0^{-1}$ , we obtain that  $\tau_0 = 16(1)$  s.

The length scale  $l_0$  was measured from weakly modulated waves in the single-wave domains; according to Eq. (1) with  $A_L = 0$ , these are related by  $A(q)^2 g_0 = \mu^2 c_1^2$ . Plotting these values we obtain Fig. 3(b), in which we recognize the quadratic behavior of  $A^2$  as a function of  $q$ . The measured  $l_0$  differed slightly (but not systematically) from run to run and from a series of such measurements and thus we end for the correlation length

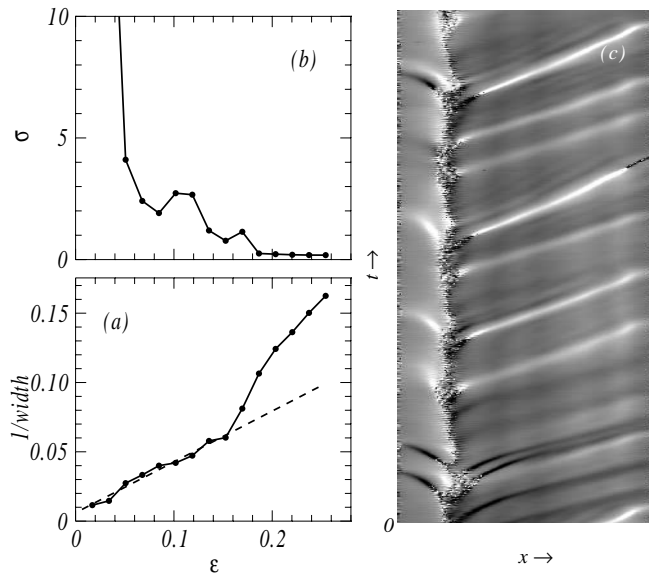


FIG. 4: (a) Dependence of the width of a source on the reduced control parameter  $\varepsilon$ . Dots: mean width  $hw_i^{-1}$ , dashed line:  $\propto \varepsilon^{-1}$ . (b) Dependence of the modulation  $\sigma = \frac{\langle l/w_i \rangle}{\langle w^2 \rangle} / \langle w \rangle^2$  of the width of a source on  $\varepsilon$ . Notice that the source becomes unstable for  $\varepsilon > \varepsilon_{ca}$ . Note that in (a)–(b), length scales have been non-dimensionalized by the characteristic scale  $\lambda_0$ . (c) Space-time diagram of the wave number field  $q(x;t)$  of an unstable source,  $\varepsilon = 0.11$ ; the extent of the  $x$  axis is  $158 \lambda_0$ , the total time is  $660 \lambda_0$ .

$\lambda_0 = (2.7 \pm 0.6) \cdot 10^3$  m, which only close to threshold becomes similar to the basic wavelength of the traveling waves.

Taking these time and length scales and the measured front velocity  $v_{E0}$  used before, we find then that  $(1 + \frac{c_1^2}{c_2^2}) = 2.6$ , from which it follows that  $c_1 = 1.3(4)$ . A weak consistency check is that  $1 + \frac{c_1^2}{c_2^2}$  should be larger than one; independent measurements of  $c_1$  would lead to a stronger consistency check.

#### IV. COMPARISON BETWEEN EXPERIMENT AND THEORY

##### A. Sources

Now that all relevant parameters of the amplitude equations are approximately known, we turn to the behavior of sources in our experiment. The dependence of the width  $w(t)$  of sources on the control parameter  $\varepsilon$  was measured in long experimental runs in which a source was located at large heating power  $\varepsilon = 0.3$  and then followed at progressively smaller values of  $\varepsilon$  [18]. At each  $\varepsilon$ , the source was observed for several hours by scanning the fluid surface, while keeping the experimental conditions constant.

From the width  $w(t_i)$  at discrete scan times  $t_i$  we computed the mean  $hw_i$  (as well as the standard deviation

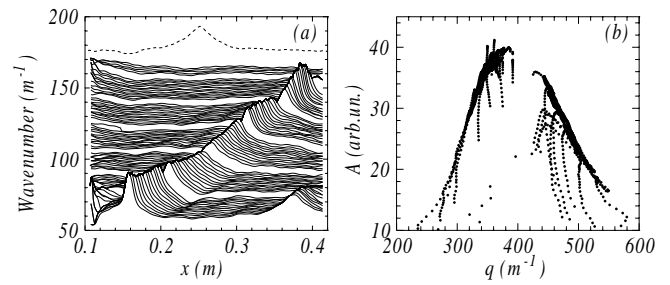


FIG. 5: (a) Wave number profile of a hole emitted from the unstable source of Fig. 4b. Dashed line: typical wave number profile. To help reading wave number on the vertical axis, the plot has been sectioned. (b) Scatter-plot of the minimum of the modulus versus the extreme (in  $x$ ) of the wave number along each of the holes shown in Fig. 4b. Both compression (large  $q$ ) and dilation (small  $q$ ) holes belong to a one-parameter family.

[18]). Fig. 4 shows that the behavior of  $hw_i$  as a function of  $\varepsilon$  in the experiments shows the same qualitative features as the numerical simulations of Fig. 2: For decreasing  $\varepsilon$  the width appears to diverge, but at  $\varepsilon = 0.15$  there is a cross-over to a  $hw_i \propto \varepsilon^{-1}$  behavior. Below this crossover value, the sources fluctuate strongly and the standard deviation of the width rapidly increases [17]. In a cyclic fashion, these sources first grow and spawn outward-spreading wave fronts, leaving an interval of near-zero wave amplitude behind in the source core. Here phase slips occur, which make the fronts jump back; the resulting phase twists are carried away by hole structures which travels roughly with the group velocity (the light and dark lines). In our numerical simulations of the coupled CGL equations (Fig. 2) exactly the same hole structures are observed. The crossover value for  $\varepsilon_{c0}^{sc}$  is consistent with the transition value  $\varepsilon_{ca}$  that we determined before.

##### B. Holes

The structures sent out by the erratic sources display a dip in the amplitude  $A$  and are therefore referred to as holes. It is well known that holes play an important role in the dynamics of traveling wave systems, and that different types can be distinguished by whether the wave numbers of their two adjacent waves are similar or substantially different [2, 3, 7, 8, 11]. From the measured wave number profile in Fig. 5a it can be seen that the wave numbers at the back and front side of the hole are very similar. We therefore associate these holes with so-called homoclinic holes [3]. In addition, they display the following typical homoclinic hole behavior (see Fig. 2b and 4b): they do not send out waves and occur quite close together, they can evolve to defects and their propagation velocity (which in lowest order is given by  $s_0$ ) depends on the value of the extremum of  $q$ . In the lo-

cal wave number plot of Fig. 2 dilation holes (the dark lines) have a larger velocity than compression holes (light lines), just as in the experimental plot Fig. 4c. In fact, the correlation between the type of wave number modulation and the velocity of these coherent structures depends on the sign of  $c_1$ , which was selected accordingly for the numerical simulations.

Since homoclinic holes are dynamically unstable, their local profiles slowly evolve along a one-parameter family; on a scatter plot of the values of the minimum of  $\mathcal{A}$  versus the corresponding extremum of  $q$ , these values collapse on a single curve [3]. The holes in our experiment precisely show this behavior: The extrema of  $\mathcal{A}$  and  $q$  rapidly evolve toward a parabolically shaped curve, and stay there during their further evolution (Fig. 5b). We only observed these holes in our experiment for at most a few characteristic times — too short to see clear signs of the weak instability predicted from the CGL equation.

## V. DISCUSSION AND OUTLOOK

Our experiments raise a number of suggestions for further work. (i) The width where sources start to fluctuate

is larger in the theory ( $O(100 \lambda_0)$ ) than in experiments ( $O(20 \lambda_0)$ ), while the fluctuations appear stronger for experimental sources. Experimental noise or non-adiabatic effects which perturb the fronts may play a role here. (ii) Earlier experiments [12] have shown that for different heights of the wire, qualitatively different behavior occurs. Systematic measurements of the coefficients as a function of height may turn the heated wire experiment into a CGL-machine with tunable coefficients. (iii) Longer observations and more controlled generation of holes may shed more light on their relation to the homoclinic holes predicted by theory, and may show the highly characteristic divergence of lifetime as a function of initial condition [3]. (iv) Sinks show non-adiabatic phase-matching and in fact possess completely anti-symmetric profiles [7]; there is no clear theoretical understanding of this.

Acknowledgment We thank Ad Holten and Gerald Oerlemans for technical assistance. Financial support by EC Network Contract FM RX-CT 98-0175, by the "Nederlandse Organisatie voor Wetenschappelijk Onderzoek (NWO)" and by "Stichting Fundamenteel Onderzoek der Materie (FOM)" is gratefully acknowledged.

- 
- [1] M. C. Cross and P. C. Hohenberg, *Rev. Mod. Phys.* 65, 851 (1993).
- [2] H. Chate, *Nonlinearity* 7, 185 (1994).
- [3] M. van Hecke, *Phys. Rev. Lett.* 80, 1896 (1998); M. van Hecke and M. Howard, *Phys. Rev. Lett.* 86, 2018 (2001).
- [4] M. van Hecke, C. Storm and W. van Saarloos, *Physica D* 134, 1 (1999).
- [5] V. Croquette and H. Williams, *Phys. Rev. A* 39, 2765 (1989).
- [6] Y. Liu and R. E. Ecke, *Phys. Rev. E* 59, 4091 (1999).
- [7] J. Burquete, H. Chate, F. Daviaud and N. Mukolobwe, *Phys. Rev. Lett.* 82, 3252 (1999).
- [8] P. Bot and I. Mutabazi, *Eur. Phys. J. B.* 13, 141 (2000).
- [9] A. Joets, R. Ribotta, *Phys. Rev. Lett.* 60, 2164 (1988); M. Rabaud, S. Michalland, Y. Couder, *Phys. Rev. Lett.* 64, 184 (1990); P. Habdas, M. J. Case, and J. R. de Bruyn, *Phys. Rev. E* 63 066305 (2001).
- [10] N. Garnier, A. Chaudel, *Phys. Rev. Lett.* 86, 75 (2001); N. Garnier, A. Chaudel, F. Daviaud, submitted to *Physica D*.
- [11] W. van Saarloos and P. C. Hohenberg, *Physica D* 56, 303 (1992).
- [12] J. M. V. Ince and M. Dubois, *Europhys. Lett.* 20, 505 (1992); *Physica D* 102, 93 (1997).
- [13] The definition of sources and sinks involves the fully nonlinear group-velocity [4], but in our experiments, the direction of this group velocity is equal to the direction of the linear group-velocity  $s_0$  (Eq. (1-2)).
- [14] P. Coulet, T. Frisch and F. P. Laza, *Physica D* 62, 75 (1993).
- [15] A. Couairon and J. M. Chomaz, *Physica D* 108, 236 (1997); S. M. Tobias, M. R. E. Proctor and E. K. Knobloch, *Physica D* 13, 43 (1998).
- [16] The brand name of the oil is Tegiloxan 3, produced by Goldschmidt AG (Essen, Germany). At 21 °C it has viscosity  $\eta = 3.397 \cdot 10^{-6} \text{ m s}^{-2}$ , density  $\rho = 892.4 \text{ kg m}^{-3}$ , surface tension  $\sigma = 18.3 \cdot 10^{-3} \text{ N m}^{-1}$ , with temperature coefficient  $d\sigma/dT = -9.7 \cdot 10^{-5} \text{ N m}^{-1} \text{ K}^{-1}$ , and a refractive index  $n = 1.395$ .
- [17] L. Pastur, M. T. Westra and W. van de Water, submitted to *Physica D*.
- [18] To quantify the width of sources we use our finding that the envelope of the experimental pattern is well fitted by the expression  $S_+(x-x_0) + S_-(x-x_0)$ , with  $S_\pm / (1 + a \exp(-2bx))^{1=2}$ . The source width  $w$  was defined as  $S_\pm(w=2) = 1=2$ .